Supporting Information

Intrinsic mixed Bloch-Néel character and chirality of skyrmions in asymmetric epitaxial trilayers

Pablo Olleros-Rodríguez[┼], Ruben Guerrero[┼], Julio Camarero[┼,ǂ], Oksana Chubykalo-Fesenko[†,*] and Paolo Perna[┼,*]

[┼] *IMDEA Nanociencia, c/ Faraday 9, Campus de Cantoblanco, 28049 Madrid, Spain.*

[ǂ] *Departamento de Física de la Materia Condensada, Instituto "Nicolás Cabrera" and Condensed Matter Physics Center (IFIMAC), Universidad Autónoma de Madrid, Campus de Cantoblanco, 28049 Madrid, Spain.*

[†] *Materials Science Institute of Madrid (ICMM-CSIC), Campus de Cantoblanco, 28049, Madrid, Spain.*

[*]*Corresponding Authors: oksana@icmm.csic.es, paolo.perna@imdea.org*

1. Spin reorientation transition.

In the study of the Spin Reorientation Transition (SRT) in Figure 3 of the main text, we have introduced inhomogeneities as fluctuations of the uniaxial anisotropy definition along 80 different regions (with an average area of 6.4 nm^2 corresponding to ~1 % of the total sample area) of the top Gr/Co monolayer. The implemented fluctuations affect both the uniaxial anisotropy constant K_U and the uniaxial anisotropy direction given by their polar and azimuthal angles θ_U and φ_U. In each region, the anisotropy constant was distributed uniformly with a 10% variation, and the anisotropy easy axis directions was varied with the polar angle following a normal distribution with a standard deviation of 0.5º and the azimuthal angle distributed uniformly within the whole plane.

If a highly-idealized system is considered, i.e. without defects or inhomogeneities, we obtain an abrupt magnetization transition from a saturated out-of-plane (OOP) to a saturated in-plane (IP) state since the ferromagnetic layer behaves as a macrospin. The comparison between the two cases is shown in Figure S1.
Note that, contrarily to the Figure 3 of the main text, we have plotted the OOP component of the magnetization normalized to its saturation value (i.e., M_Z/M_S) to highlight the transition region.

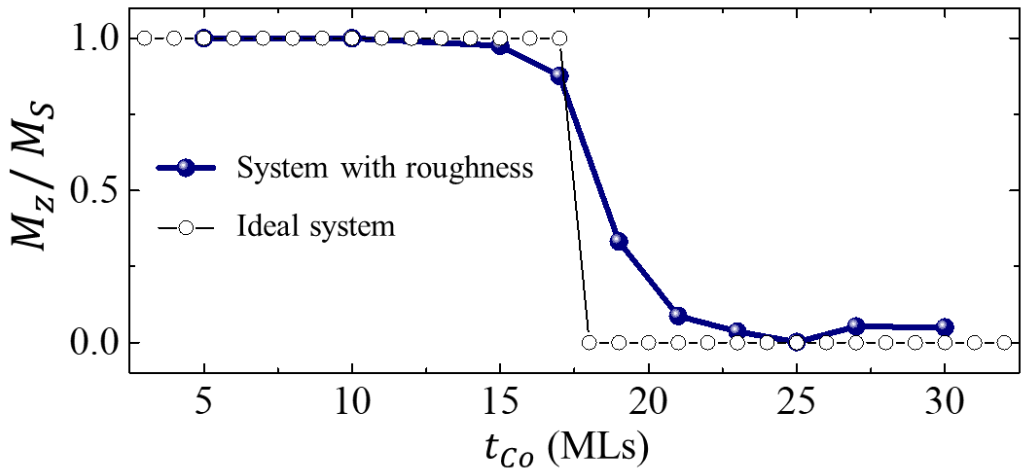

Figure S1. Spin Reorientation Transition. The Spin Reorientation Transition for the ideal case (empty dots), and for the case in which the inhomogeneities in the Co monolayer in contact with Graphene have been introduced by defining fluctuations of the uniaxial anisotropy as explained in the text (blue dots). M_Z is the out-of-plane magnetization component normalized to the saturation M_S.

2. Dependence on the initial magnetization configuration in nanodots

As discussed in the manuscript, the initial magnetization configuration from which the presented results are obtained is defined as a step function along the radial coordinate:

$$m_Z(\rho) = \begin{cases} -1;\ \forall\rho \leq \frac{R_{DOT}}{2} \\ 1;\ \forall\rho > \frac{R_{DOT}}{2} \end{cases} \quad (1)$$

In which ρ is the radial direction, $m_Z(\rho)$ is the OOP component of the magnetization and R_{DOT} is the dot radius.

With this definition, the magnetization at the core of the dot points antiparallel (along the OOP direction) with respect to the shell, which points upwards (inverted core state, ICS). In such a way, we avoid the imposition of a certain chirality to the domain wall of the initial skyrmion state. In order to study the dependence of the final states on the initial ones, we carried out a series of simulations for selected Co thicknesses (i.e. t_{Co} =18, 26 and 30 MLs) in which the initial configurations were defined as Bloch skyrmions with CW or CCW configurations. Such initial configurations are sketched in top panel of **Figure S2**. The OOP magnetization profiles of the final states obtained starting from ICS state (circles), Bloch- CCW (blue line) and Bloch-CW skyrmion (red line) are shown in the main panel of **Figure S2**.

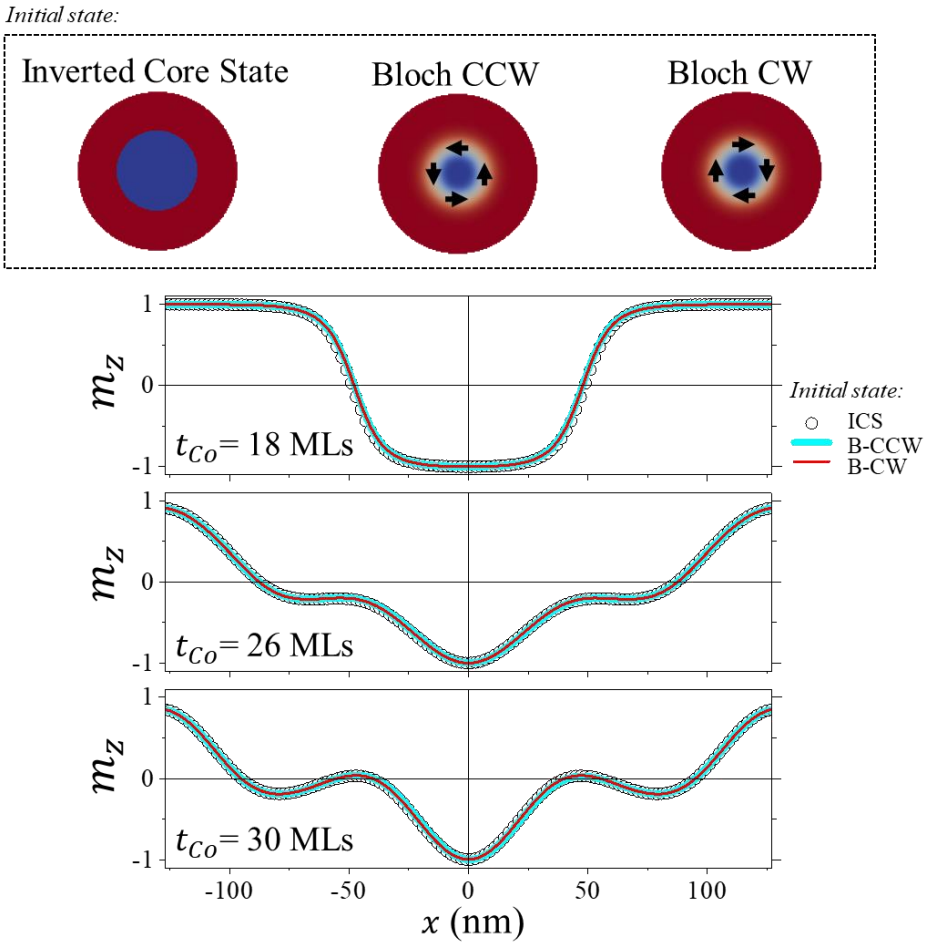

Figure S2. Initial state configurations and final m_z profiles. Top panel: sketches of the inverted core state (ICS, dots), Bloch-CCW (B-CCW, blue line) and Bloch-CW (B-CW, red line) skyrmion initial configurations. Main panel: profile of m_z along the x-direction for the three initial states.

The results demonstrate that for all the initial definitions the system evolves towards the same OOP magnetization profile (i.e. $m_Z(\rho)$).

The IP components of the magnetization, i.e. $m_\rho(\rho)$ and $m_\varphi(\rho)$, are presented in **Figure S3**.

We can observe two different behaviors:

i) the chirality of the Néel contribution, $m_\rho(\rho)$ in panel a, is independent of the initial state assuming always a final CCW chirality. This behavior is due to the sign of the DMI, which is always positive.

ii) the chirality of the Bloch contribution, $m_\varphi(\rho)$ in panel b, depends on the initial configuration, being CW (CCW) depending on the initial CW (CCW) skyrmion chirality. This is because DMI is not strong enough to overcome the energy barrier separating the CW and CCW states. [1]

Apart from the chirality, the Bloch contribution shows the same shape independently from the initial contribution (in panel b, red dashed line refer to $-m_\varphi(\rho)$). The Néel contribution (panel a) does not substantially change as well.

Apart from this qualitative and quantitative analysis of the OOP and IP magnetization profiles, we computed the energies of the final magnetic states. The resulting energies show that the different stable or metastable states (see manuscript) obtained with different initial configurations converge to the same energy.

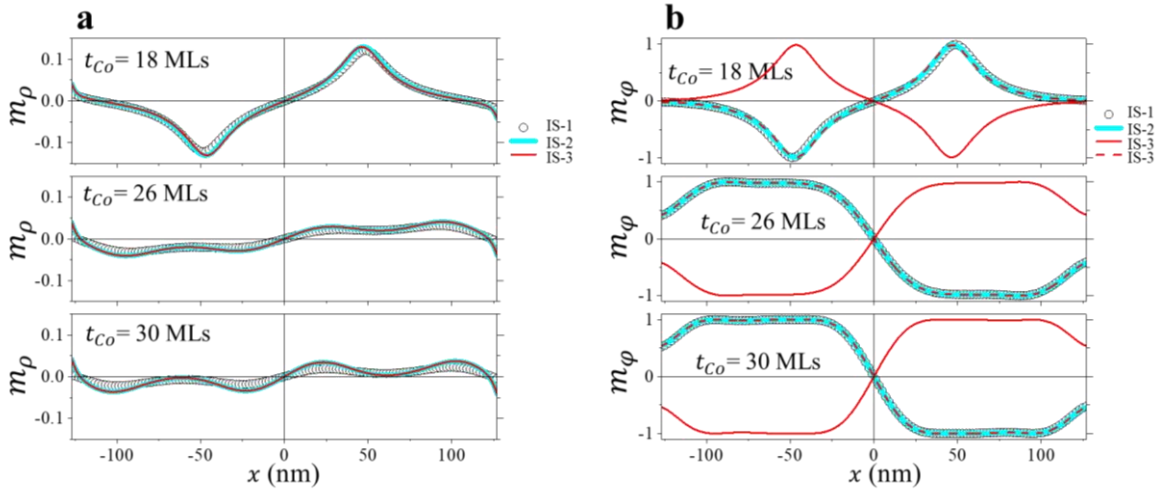

Figure S3. Final m_ρ and m_φ profiles. Panel a: m_ρ along the x-direction of the final states starting from single core domain (SCD, dots), Bloch-CCW (B-CCW, blue line) and Bloch-CW (B-CW, red line) skyrmion initial configurations. Panel a: m_φ along the x-direction of the final states starting from single core domain (SCD, dots), Bloch-CCW (B-CCW, blue line) and Bloch-CW (B-CW, red line) skyrmion initial configurations (in panel b, red dashed line refer to $-m_\varphi(\rho)$).

3. Magnetization profiles in nanodots as function of Co thickness.

From the analysis of the skyrmions m_z profiles in the nanodots as function of the Cobalt thickness (t_{Co}) we notice that for $t_{Co} > 22$ MLs, two different pseudo domains are created inside the DW, and the skyrmions profiles present a complex behavior. In the specific case of 26 MLs (red curve in panel a of Figure 5), we even observed a change of the slope sign along the skyrmion profile. This behavior is due to the creation of a new DW. In addition, at 30 MLs, the magnetization between the core and the shell of the skyrmion takes both positive and negative values displaying a wave-like spin behavior in the final state. Only for thinner film, i.e. $t_{Co} \leq 22$ MLs, the profiles resemble the ones of a well-defined skyrmions in the case of constant DMI along the film thickness.

There exist different analytical expressions for the description of the skyrmion profiles (i.e. $\theta_{\overline{m}}(\rho)$), as in Ref.[2] and Ref.[3] respectively:

$$\text{(Fit 1)}: m_z = cos\,\theta_{\overline{m}}(\rho) = cos\left[2atan\left(e^{P_S\frac{\rho-\rho_S(t_{Co})}{\Delta(t_{Co})}}\right)\right]$$

$$\text{(Fit 2)}: m_z = cos\,\theta_{\overline{m}}(\rho) = cos\left[2atan\left(\left(\frac{\rho_S}{\rho}\right)^{P_S} e^{P_S\frac{\rho-\rho_S(t_{Co})}{\Delta(t_{Co})}}\right)\right]$$

In which, ρ_S is the skyrmion radius, Δ is the DW width and $P_S = \pm 1$ is the polarization of the core of the skyrmion (i.e. $m_Z(\rho = 0)$) .

In **Figure S4**, it can be clearly observed that both expressions fail in reproducing the skyrmions profiles in our simulations for $t_{Co} > 22$ MLs. For thinner dots, the radius of the skyrmions increases from 48.4 nm (18 MLs) to 71.2 nm (22 MLs). The DW width also shows an increasing behavior from 18.9 nm to 42.1 nm.

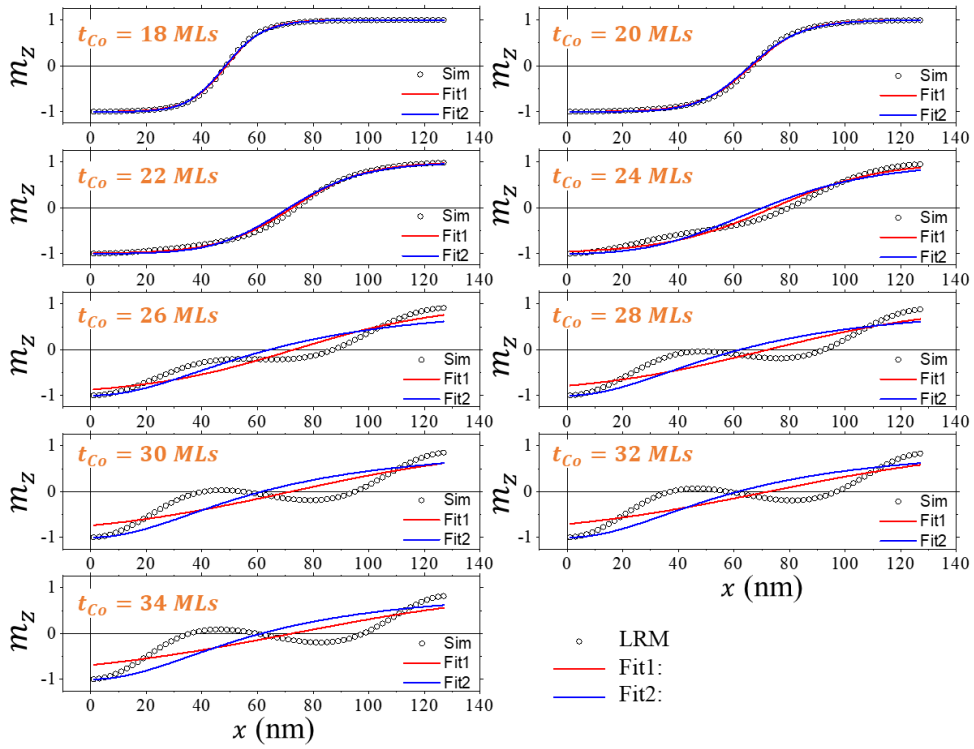

Figure S4. Skyrmion profiles in nanodot as function of the Co thickness. Plots of m_z along the radius of the dot for selected Co thickness. The symbols refer to the results of the LRM simulations, Fit 1 and Fit 2 refer instead to the analytical formulae in Ref. [2] and [3]. It is clear that these expressions do not reproduce the obtained skyrmion profiles for thicknesses larger than 22 MLs.

4. Comments on helicity.

It is possible to define the helicity parameter to describe the observed changes of the spin configuration between the Bloch and Néel states of opposite chirality. Indeed, the magnetization in the center of the DW (i.e. $m_z = 0$) can be expressed using the spherical coordinates as $\Theta(r) = \pi/2$ and $\Phi(r, \varphi) = \Phi_0 + \varphi$ where Φ_0 is the helicity or skyrmion phase and carries the information of the chiral character of the DW. The helicity takes values $\Phi_0 = +(-)\frac{\pi}{2}$ for pure CCW (CW) Bloch skyrmions and $\Phi_0 = 0(\pi)$ for pure CCW (CW) Néel-like skyrmions. In **Figure S5** it is shown the thickness dependence of the helicity. In the figure, the solid (empty) symbols refer to the two possible chirality of the Bloch component that can be obtained depending on the initial state. As it can be seen Φ_0 takes always values close to $\Phi_0 \sim \pm\frac{\pi}{2}$ showing the major Bloch contribution, which becomes more important as the t_{Co} is increased. This is an expected behavior as consequence of the reduction of the effective DMI (large DMI stabilizes Néel-type configuration). The change of the chirality of the DW is reflected as an abrupt change in the sign of Φ_0. Note that for $t_{Co} \geq 5.6\, nm$, because of the complex wavy structure of DWs, we can define three different radii, (i.e. outer, middle and inner).

However, note that the ratio (R) introduced in the main text, $R = \left.\frac{|m_\rho|}{\sqrt{m_\varphi^2 + m_\rho^2}}\right|_{m_Z=0}$ gives a more visual description of the weight of each contributions, i.e. Néel and Bloch percentage. The latter in fact is obtained by doing a transformation to spherical coordinates. Moreover, by using helicity we cannot represent the percentage contributions as function of the thickness as done in Figure 7.

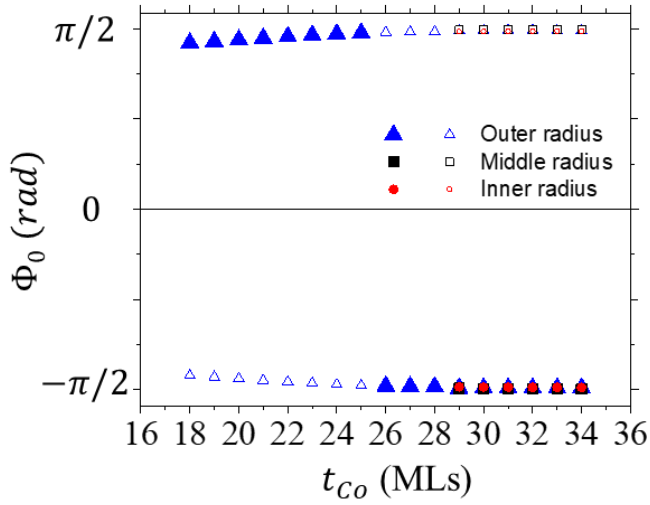

Figure S5. Thickness dependence of the helicity, Φ_0. $\Phi_0 \sim \pm\frac{\pi}{2}$ for samples with different Co thickness. This demonstrates the major Bloch contribution. The solid (empty) symbols represent the final helicity when starting from a Bloch-CCW (CW) initial state.

5. Layer Resolved Model vs. One-Layer Model

The study of the spin textures in magnetic nanodots have been carried out by using a layer resolved model (LRM) as described in the main text. Here, we compare the LRM with a micromagnetic model that consider one single cell along the OOP direction (i.e., one-layer model or 1LM) with the effective micromagnetic parameters K_{eff} and D_{eff} evaluated from Eqs.(1-2) and which depend on the thin film thickness. The in-plane discretization is the same in both models.

In **Figure S6**, symbols refer to the results of the 1LM and lines correspond to the results obtained with the LRM, at selected Co thicknesses. First, we analyse the differences in the OOP magnetization profile (panel a). In both models, skyrmions cannot survive for $t_{Co} < 18$ MLs. At $t_{Co} = 18$ MLs, the skyrmion is stabilized in both models being the skyrmion radius predicted by the 1LM 8.4% smaller than the radius predicted by the LRM (44.56 nm and 48.65 nm respectively). The skyrmion ground state is obtained by both models from t_{Co}> 18 MLs to $t_{Co} = 22$ MLs, decreasing the differences in the profile as the thickness of the dot is increased. At t_{Co}=25 MLs the OOP magnetization profile given by the 1LM (green dots) shows the change in the slope which is predicted to occur at t_{Co} =26 MLs by the LRM. At t_{Co}=27 MLs the 1LM (black dots) converges to a different state (bottom panel in Figure 6) in which the OOP component of the magnetization along the border fluctuates and takes positive and negative values. The corresponding skyrmion number (as defined in the main text) is $N_{Sk} = 0.42$ which is closer to the typical values of a vortex (i.e., 1/2) rather than that of a skyrmion (i.e., 1). We refer to this state as pseudo vortex. For thicknesses $t_{Co} \geq 28$ MLs, both models predict pseudo-skyrmions configurations showing almost the same profiles.

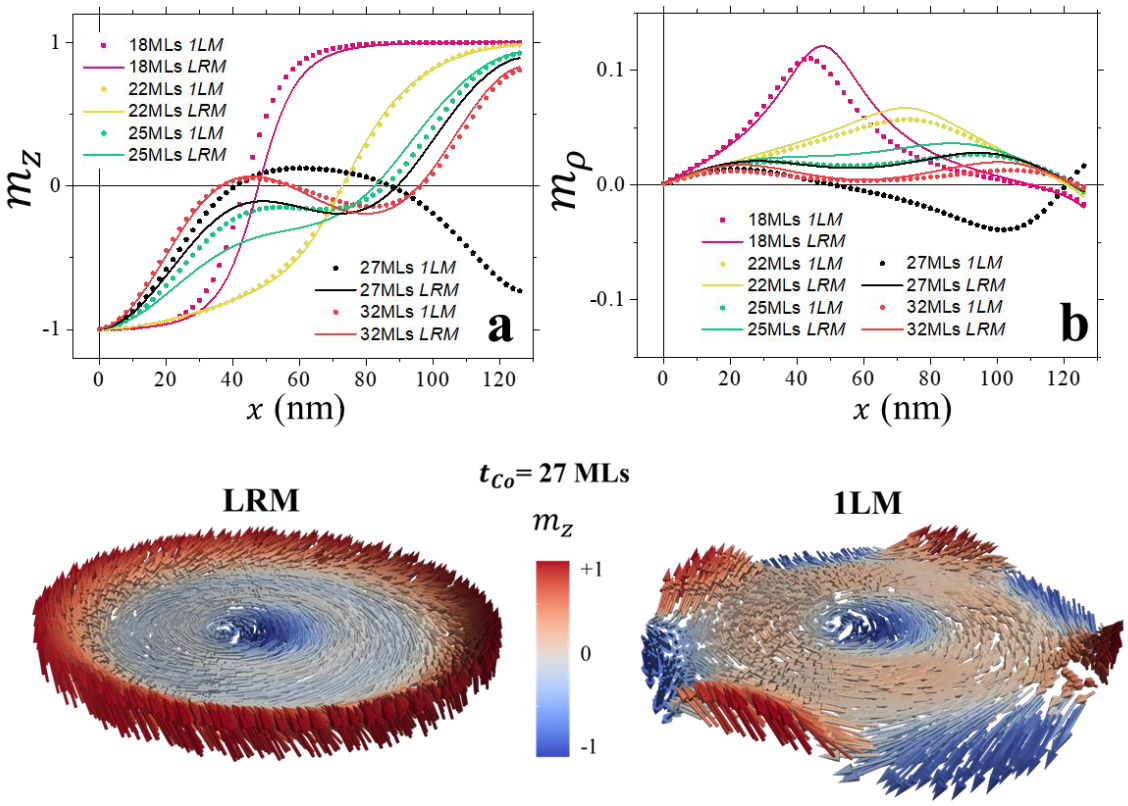

Figure S6. Comparison of the Layer-Resolved Model (LRM) versus the 1-Layer Model (1LM). Panel a) Out-of-plane magnetization profile for both, the LRM (solid lines) and the 1LM (solid symbols) at selected thicknesses. Panel b) Comparison of the profile related to the Néel contribution. The spin configurations at 27 MLs for LRM and 1LM are illustrated in the bottom panel.

The pseudo-vortex state obtained by the 1LM at $t_{Co} = 27$ MLs has been also obtained using the LRM at the same thickness and starting from an initial vortex configuration. The energy density of the system in this case is $\varepsilon_{Vortex} = 1.78$ kJ/m^3 whereas the energy density of the pseudo-skyrmion obtained at the same thickness when starting from an initial ICS state is ε_{Sk} = -0.68 kJ/m^3. Thus the pseudo-skyrmion configuration is more stable than the pseudo vortex. Moreover, such a one layer approximation produces final ground states with higher energies than the one obtained by LRM.

6. Comments on thermal stability

The thermal stability have been studied considering the Langevin dynamics given by the LLG equation including the thermal field as implemented in Mumax[3]. The simulations have been carried out during 10 ns for the nanodots with thicknesses $t_{Co} = 18$ MLs and $t_{Co} = 30$ MLs. In both cases, the initial state was set to be the final ground states obtained at their corresponding thicknesses (i.e. Skyrmion and pseudo-Skyrmion states). The resulting m_Z, m_θ and m_ρ profiles obtained each 1 ns of simulation time are presented as lines with symbols in **Figure S7**. In those plots, the black solid line represents the profile at 0 K and the green solid line represents the averaged profiles along the total simulation time. In the case of 18 MLs (panel a) we can observe that the skyrmion state is not destroyed and maintain the profiles on average. However, it can be observed that the radius of the skyrmion is incremented. For $t_{Co} = 30$ MLs (panels b) the black and green solid lines almost overlap, meaning that for large thickness the pseudo-skyrmion state is barely affected from the temperature. Snapshots of the resulting spin configuration at 10 ns for 0 K and 300 K are displayed in the bottom boxes. It can be easily observed that our skyrmions are stable states in a range of Co thickness and a large number of layers ensures their stability against thermal fluctuations.

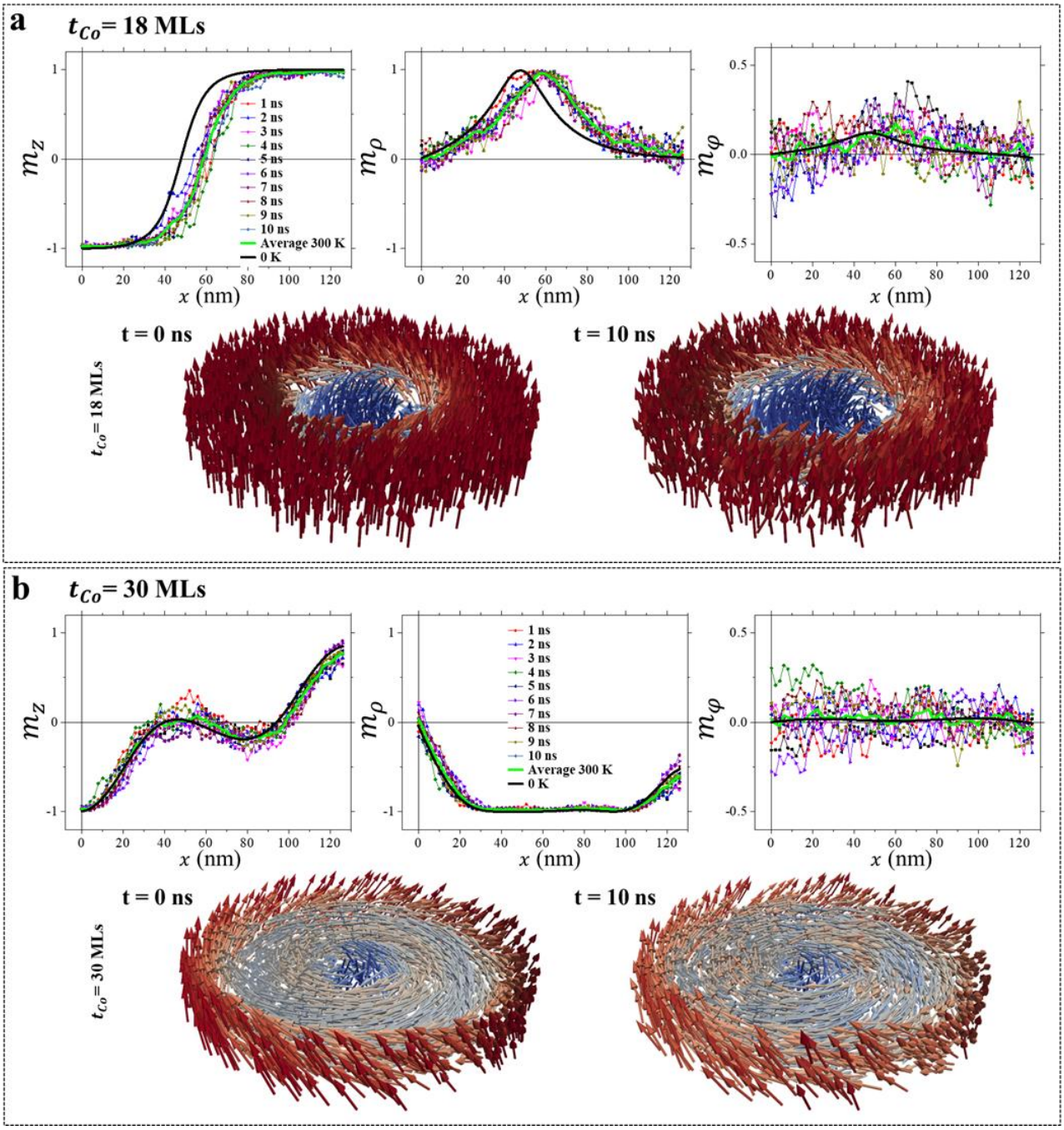

Figure S7. Thermal stability study. The thermal stability at 300 K have been studied considering the Langevin dynamics given by the LLG equation and compared to the 0 K case. The cases of $t_{Co} = 18$ MLs and 30 MLs are presented in panel a and b respectively, together with the corresponding snapshots of the resulting spin configuration at 10 ns (bottom boxes).

1. Rohart, S.; Thiaville, A. Skyrmion confinement in ultrathin film nanostructures in the presence of Dzyaloshinskii-Moriya interaction. *Physical Review B* **2013**, 88, 184422.
2. Aranda, A. R.; Hierro-Rodriguez, A.; Kakazei, G. N.; Chubykalo-Fesenko, O.; Guslienko, K. Y. Magnetic skyrmion size and stability in ultrathin nanodots accounting Dzyaloshinskii-Moriya exchange interaction. *Journal of Magnetism and Magnetic Materials* **465** (2018): 471-479.
3. Tejo, F.; Riveros, A.; Escrig, J.; Guslienko, K. Y.; Chubykalo-Fesenko, O. Distinct magnetic field dependence of Néel skyrmion sizes in ultrathin nanodots. *Scientific reports* **2018**, 8, 6280.